AIAA'89

AIAA-89-0550
Numerical Versus Physical Dissipation in the Solution of Compressible Navier-Stokes Equations

George S. Dulikravich, Daniel J. Dorney and Seungsoo Lee

The Pennsylvania State University
University Park, PA 16802

27th Aerospace Sciences Meeting
January 9-12, 1989
Reno, Nevada

NUMERICAL VERSUS PHYSICAL DISSIPATION IN THE SOLUTION OF COMPRESSIBLE NAVIER-STOKES EQUATIONS

George S. Dulikravich Daniel J. Dorney Seungsoo Lee
Associate Professor Graduate Student Graduate Student
Department of Aerospace Engineering
The Pennsylvania State University
University Park, PA 16802

ABSTRACT

Many numerical algorithms presently used for the solution of the Navier-Stokes equations of gasdynamics rely on the explicit addition of artificial dissipation terms to yield non-oscillatory results in regions containing strong flow gradients. In this investigation, the characteristics of two existing artificial dissipation models (Jameson et al and Ni) are compared with the characteristics of natural dissipation incorporated in the Navier-Stokes equations. In addition, the characteristics of the new Physically Based Dissipation (PBD) model are compared with the characteristics of the natural dissipation. Results indicate that existing artificial dissipation models can yield values of dissipation that are significantly larger in magnitude and often of opposite sign than the natural dissipation. The PBD model is shown to yield values of dissipation that more closely resemble the natural dissipation terms, thus offering an alternative approach to artificial dissipation modeling.

INTRODUCTION

When the equations of gasdynamics are solved using a central difference scheme (e.g., a Runge-Kutta time stepping scheme [1]), decoupling of odd and even grid points generates oscillations in the numerical algorithm. These oscillations can be damped by either explicitly or implicitly adding a certain amount of artificial dissipation [2].

Contemporary dissipation models for central difference schemes are intentionally [3] devoid of physics and represent an intuitive combination of second and fourth order artificial (non-physical) dissipation terms [1]. The second order artificial terms are used to damp oscillations in shock regions, while the fourth order artificial terms ensure monotonic convergence to steady state in smooth flow regions [1]. Nevertheless, different amounts of second and fourth order dissipation can produce different numerical solutions [4,5] especially in the case of transonic shocked separated flow [6,7]. The objective of this work is to compare the characteristics of the artificial dissipation models of Jameson et al [8] and Ni [3] with the characteristics of natural (physical) dissipation resulting from the Navier-Stokes equations. In addition, the characteristics of the newly developed Physically Based Dissipation (PBD) model [9,10,11] will be compared with the characteristics of the natural dissipation.

PHYSICAL DISSIPATION IN NAVIER-STOKES EQUATIONS

In the computational (ξ,η) domain, the two-dimensional Navier-Stokes equations in conservation form can be represented by:

$$\frac{\partial Q}{\partial t}+\frac{\partial E}{\partial \xi}+\frac{\partial F}{\partial \eta}=\frac{1}{R_e}\left(\frac{\partial E^v}{\partial \xi}+\frac{\partial F^v}{\partial \eta}\right) \tag{1}$$

where

$$Q = J\begin{bmatrix}\rho\\ \rho u\\ \rho v\\ \rho e_o\end{bmatrix}$$

$$E = \begin{bmatrix}\rho U\\ \rho uU + y_\eta\, p/J\\ \rho vU - x_\eta\, p/J\\ \rho U h_o\end{bmatrix}$$

$$F = \begin{bmatrix}\rho V\\ \rho uV - y_\xi p/J\\ \rho vV + x_\xi p/J\\ \rho V h_o\end{bmatrix} \tag{2}$$

Here, ρ is the density, p the thermodynamic pressure, u,v the Cartesian velocity components, e_o the total mass-specific energy and h_o the total mass-specific enthalpy. R_e is the Reynolds number, while E^v and F^v incorporate physical dissipation terms due to shear viscosity, μ, secondary viscosity, λ, and heat conduction, k. Thus, the physical dissipation flux vectors are:

$$E^v = \begin{bmatrix} 0 \\ (y_\eta \tau_{xx} - x_\eta \tau_{xy})/J \\ (y_\eta \tau_{xy} - x_\eta \tau_{yy})/J \\ (y_\eta B_x - x_\eta B_y)/J \end{bmatrix}$$

$$F^v = \begin{bmatrix} 0 \\ (x_\xi \tau_{xy} - y_\xi \tau_{xx})/J \\ (x_\xi \tau_{yy} - y_\xi \tau_{xy})/J \\ (x_\xi B_y - y_\xi B_x)/J \end{bmatrix} \qquad (3)$$

The contravariant velocity components are:

$$U = (uy_\eta - vx_\eta)/J \; ; \quad V = (vx_\xi - uy_\xi)/J \qquad (4)$$

and the Jacobian of the transformation matrix is:

$$J = x_\xi y_\eta - x_\eta y_\xi \quad ; \quad \xi_x = \frac{y_\eta}{J} \; ; \; \xi_y = -\frac{x_\eta}{J} \; ;$$

$$\eta_x = -\frac{y_\xi}{J} ; \; \eta_y = \frac{x_\xi}{J} \qquad (5)$$

The shear stress terms are:

$$\tau_{xx} = \mu'' u_x + \lambda v_y = [\mu''(u_\xi y_\eta - u_\eta y_\xi) + \lambda(v_\eta x_\xi - v_\xi x_\eta)]/J \qquad (6)$$

$$\tau_{yy} = \mu'' v_y + \lambda u_x = [\mu''(v_\eta x_\xi - v_\xi x_\eta) + \lambda(u_\xi y_\eta - u_\eta y_\xi)]/J \qquad (7)$$

$$\tau_{xy} = \mu (u_y + v_x) = \mu (u_\eta x_\xi - u_\xi x_\eta + v_\xi y_\eta - v_\eta y_\xi)/J \qquad (8)$$

and the energy parameters are:

$$B_x = u\tau_{xx} + v\tau_{xy} + \frac{\mu}{(\gamma-1)M_\infty^2 P_r}(T_\xi y_\eta - T_\eta y_\xi)/J \qquad (9)$$

$$B_y = u\tau_{xy} + v\tau_{yy} + \frac{\mu}{(\gamma-1)M_\infty^2 P_r}(T_\eta x_\xi - T_\xi x_\eta)/J \qquad (10)$$

Here, μ'' is the longitudinal viscosity coefficient ($\mu'' = 2\mu + \lambda$). Also, M_∞ is the freestream Mach number, Pr is the Prandtl number and T is the absolute temperature. Since Rankine-Hugoniot shock jump conditions are guaranteed only if Stokes hypothesis ($\lambda/\mu = -2/3$) is enforced [12,13], this relation was used in actual computations.

PHYSICALLY BASED (ARTIFICIAL) DISSIPATION

In an effort to make the dissipation terms more closely resemble physical dissipation, we introduce the concept of Physically Based Dissipation (PBD). The idea [9] is to use the right-hand side of the Navier-Stokes equations (eq. 3) as the basis for artificial dissipation, while retaining slip boundary conditions when using it in the Euler equations. In addition, the viscosity coefficient, μ, should be allowed to vary throughout the flowfield according to an "artificial dissipation sensor". For the purpose of this study, the "artificial dissipation sensor" will be based on the first derivative of pressure, which is explicitly found in the equations of motion. Nevertheless, a number of other possibilities exist for choosing an appropriate "artificial dissipation sensor" [9,11].

We propose a linear combination of the physical shear viscosity coefficient, μ, and the related artificial dissipation in order to create a physically based artificial dissipation model for the Navier-Stokes equations

$$\mu_{PBD} = \mu + \mu \, C \, \frac{|p_{i+1} - p_i|}{p_{i+1} + p_i} \qquad (11)$$

This model is reminiscent of the well known "turbulent viscosity" coefficient formulation. Here, C is a single user specified constant. We used C=14 in all the test cases. Notice that the PBD model for Navier-Stokes equations uses exactly the same derivatives of the velocity vector components as they appear in the actual stress terms of the Navier-Stokes equations. Since μ_{PBD} is always positive, it follows that the PBD model should produce non-negative entropy thus satisfying the second law of thermodynamics. We note that using the PBD model in both Euler and in Navier-Stokes equations leaves the continuity equation intact (i.e. the right-hand side equals zero), while the conventional artificial dissipation models alter the right hand side of the continuity equation. In addition, the use of the PBD model allows

an Euler solver to be easily converted to a Navier-Stokes solver [9,10].

EXISTING ARTIFICIAL DISSIPATION MODELS

When using central difference schemes to obtain numerical solutions to equation (1), the flow solution can decouple at odd and even grid points. Consequently, some form of artificial dissipation must be introduced to obtain stable solutions. Thus, the modified set of equations is

$$\frac{\partial Q}{\partial t} + \frac{\partial E}{\partial \xi} + \frac{\partial F}{\partial \eta} = \frac{1}{R_e}\left(\frac{\partial E^v}{\partial \xi} + \frac{\partial F^v}{\partial \eta}\right) + d(Q) \tag{12}$$

where $d(Q)$ is an artificial dissipative operator.

In the artificial dissipation model made popular by Jameson et al [1], the calculations of all the artificial dissipation terms are done similarly. The dissipation is defined in the computational domain as:

$$d(Q) = d_\xi Q + d_\eta Q \tag{13}$$

where Q is defined in equation (1). The terms $d_\xi Q$ and $d_\eta Q$ are contributions from the two computational coordinate directions. Then

$$d_\xi Q = d_{i+1/2,j} - d_{i-1/2,j} \; ; \; d_\eta Q = d_{i,j+1/2} - d_{i,j-1/2} \tag{14}$$

The terms on the right-hand side of equations (14) are similar. For example

$$d_{i+1/2,j} = \frac{J_{i+1/2,j}}{\Delta t}\{\epsilon^{(2)}_{i+1/2,j}(Q_{i+1,j} - Q_{i,j}) + \epsilon^{(4)}_{i+1/2,j}(Q_{i+2,j} - 3Q_{i+1,j} + 3Q_{i,j} - Q_{i-1,j})\} \tag{15}$$

where $\epsilon^{(2)}$, $\epsilon^{(4)}$ are flow adaptive coefficients that are defined as:

$$\epsilon^{(2)} = \kappa^{(2)} \max(\nu_{i+1,j}, \nu_{i,j}) \tag{16}$$

$$\epsilon^{(4)} = \max(0, (\kappa^{(4)} - \epsilon^{(2)}_{i+1/2,j})) \tag{17}$$

and the "artificial dissipation sensor" is

$$\nu_{i,j} = \frac{|p_{i+1,j} - 2p_{i,j} + p_{i-1,j}|}{p_{i+1,j} + 2p_{i,j} + p_{i-1,j}} \tag{18}$$

where the two user specified constants are

$$k^{(2)} = 1/4 \qquad k^{(4)} = 1/256 \tag{19}$$

The artificial dissipation model suggested by Ni is defined as:

$$d(Q) = \mu_{NI}(Q_{i,j} - Q_{i,j}) \tag{20}$$

where

$$Q = \frac{1}{4}[Q_{i+1,j+1} + Q_{i+1,j-1} + Q_{i-1,j+1} + Q_{i-1,j-1}] \tag{21}$$

and

$$\mu_{NI} = \sigma\left(\frac{\Delta t}{\Delta x} + \frac{\Delta t}{\Delta y}\right) \tag{22}$$

Here, σ is an artificial damping factor. We used the value $\sigma = 1.5$ in all the test cases.

COMPARISON FORMULATION

Subsonic and supersonic inlet flow cases were investigated for flow through a two dimensional contracting nozzle. The sign and magnitude of the artificial dissipation terms generated by each artificial dissipation model were compared to the dissipation generated by the physical terms in the Navier-Stokes equations.

The various artificial dissipation models were compared to the Navier-Stokes dissipation by calculating the dissipation that they generate at cell centers. Thus,

$$\bar{D}_{JAM} = \frac{D_{Jameson}}{D_{Navier\text{-}Stokes}}$$

$$\bar{D}_{NI} = \frac{D_{NI}}{D_{Navier\text{-}Stokes}}$$

$$\bar{D}_{PBD} = \frac{D_{PBD}}{D_{Navier\text{-}Stokes}} \tag{23}$$

For example, if one considers only the dissipation in the x-momentum equation, and only from the ξ direction, then

$$D_{Jameson} = \frac{J_{i+3/2,j}}{\Delta t}\left(\epsilon^{(2)}_{i+3/2,j}\left[(\rho u)_{i+2,j} - (\rho u)_{i+1,j}\right]\right.$$

$$\left.-\epsilon^{(4)}_{i+3/2,j}\left[(\rho u)_{i+3,j} - 3(\rho u)_{i+2,j} + 3(\rho u)_{i+1,j} - (\rho u)_{i,j}\right]\right)$$

$$- \frac{J_{i+1/2,j}}{\Delta t}\left(\epsilon^{(2)}_{i+1/2,j}\left[(\rho u)_{i+1,j} - (\rho u)_{i,j}\right]\right.$$

$$\left.-\epsilon^{(4)}_{i+1/2,j}\left[(\rho u)_{i+1,j} - 3(\rho u)_{i+1,j} + 3(\rho u)_{i,j} - (\rho u)_{i-1,j}\right]\right) \quad (24)$$

$$D_{NI} = (\mu_{NI})_{i+1,j}\left(\frac{1}{4}\left[(\rho u)_{i+2,j+1} + (\rho u)_{i+2,j-1}\right.\right.$$

$$\left.\left. + (\rho u)_{i,j+1} + (\rho u)_{i,j-1}\right] - (\rho u)_{i+1,j}\right)$$

$$- (\mu_{NI})_{i,j}\left(\frac{1}{4}\left[(\rho u)_{i+1,j+1} + (\rho u)_{i+1,j-1}\right.\right.$$

$$\left.\left. + (\rho u)_{i-1,j+1} + (\rho u)_{i-1,j-1}\right] - (\rho u)_{i,j}\right) \quad (25)$$

$$D_{PBD} = \left(\frac{y_\eta \tau_{xx} - x_\eta \tau_{xy}}{J}\right)^{PBD}_{i+1,j} - \left(\frac{y_\eta \tau_{xx} - x_\eta \tau_{xy}}{J}\right)^{PBD}_{i,j} \quad (26)$$

$$D_{Navier\text{-}Stokes} = \left(\frac{y_\eta \tau_{xx} - x_\eta \tau_{xy}}{J}\right)_{i+1,j} - \left(\frac{y_\eta \tau_{xx} - x_\eta \tau_{xy}}{J}\right)_{i,j} \quad (27)$$

In the eq. 26 the viscosity coefficient is varied according to eq. 11. Eq. 27 was computed using the physical values for μ and the velocity derivatives obtained from the solution of the Navier-Stokes equations. In actual calculations, the ratios of the dissipative terms (Eq. 23) contain components from both the ξ and η directions.

RESULTS

Two grids were used to discretize the nozzle: a coarse 40x20, clustered grid (Figure 1), and a finer 80x40, strongly clustered grid (Figure 2). On both grids, the top of the grid represents a solid wall, while the bottom of the grid represents the line of symmetry for the nozzle. The inlet is at the left of the grid, while the outlet is at the right of the grid. Flow boundary conditions at these boundaries were enforced using Riemann invariants. A no-slip condition was used on the upper wall and the reflection condition was used on the lower wall. All internal flow cases considered were run using the same basic code for 1700 iterations on a Vax 8600 computer starting with the identical initial guess of a uniform flow field.

The first test case considered was for an inlet Mach number of 0.6 and a Reynolds number of 100,000. Figures 3-10 show the ratios of the Jameson's, Ni's and PBD dissipation, with respect to the physical dissipation in the Navier-Stokes equations on coarse and clustered fine grids. In all figures, DA/DN is the ratio (Eq. 23) of the value from the given artificial dissipation model to the value from the Navier-Stokes equations. For the x-momentum equation, Figure 3 shows the ratios along the grid line mid-way between the lower and upper boundary and Figure 4 shows the ratios along the upper wall. Jameson's artificial dissipation is seen to be orders of magnitude larger than the Navier-Stokes dissipation. At the upper wall, not only are Jameson's artificial dissipation terms larger in magnitude, but in many locations this dissipation also has the wrong sign thus effectively creating a negative entropy. Even though Jameson's dissipation terms may locally have the wrong sign, global convergence is still achieved since this formulation also produces exceedingly large positive dissipation at other locations. Similar results for Jameson's dissipation appear in the energy equation. Results from using Ni's dissipation show that it is uniformly of the proper magnitude and sign. This is expected since Ni's dissipation is actually a form of residual smoothing. Results using Physically Based Dissipation indicate that it is of the correct sign and that it varies monotonically.

The second test case was for an inlet Mach number of 0.9. Figures 11-18 show the results for x-momentum and energy equation dissipation ratios on coarse and fine grids. Jameson's artificial dissipation is often considerably larger in magnitude and in many cases has the opposite sign of the Navier-Stokes dissipation. Physically Based Dissipation has the correct sign although somewhat higher magnitude than the Navier-Stokes dissipation. Ni's artificial dissipation again seems to be closest to the Navier-Stokes physical dissipation.

Figures 19-26 illustrate results for the x-momentum equation dissipation ratios on coarse and fine grids for supersonic inlet flow with $M_\infty = 1.2$. Note that Jameson's artificial dissipation is highly oscillatory and generally of the wrong magnitude and the opposite sign of the Navier-Stokes dissipation. The supersonic

results with Jameson's artificial dissipation used only second order dissipation, since introduction of the fourth order artificial dissipation consistently caused the algorithm to diverge. Also, the coefficient $\epsilon^{(2)}$ had to be decreased by 50% from $M_\infty = 0.6$ to $M_\infty = 1.2$ test case.

Field plots of constant pressures obtained using the three artificial dissipation formulations are presented in Figures 27-29 indicating a considerably thicker boundary layer obtained with the Jameson's artificial dissipation.

In order to demonstrate the applicability of the PBD formulation to Euler equations of inviscid gasdynamics, a transonic flow ($M_\infty = 0.5$) about a circle (Fig. 30) was computed. Jameson's artificial dissipation caused strong inviscid separation (Fig. 31) while PBD scheme generated a barely noticeable (Fig. 32) trailing edge separation which is in agreement with the TVD type artificial dissipation schemes [6,7]. This strong influence of artificial dissipation models on inviscid separation is also visualized in Fig. 33-34 depicting the computed streamline pattern.

CONCLUSIONS

Three artificial dissipation models have been discussed and compared to the natural dissipation obtained from the Navier-Stokes equations. It was found that the artificial dissipation of Jameson et al has often the wrong magnitude and the opposite sign of the physical dissipation. The artificial dissipation of Ni is consistent with the signs and magnitudes of the physical dissipation which may be due to the fact that it is based on residual smoothing. The Physically Based Dissipation formulation is introduced as an alternative to the existing artificial dissipation schemes. It appears to be consistent with the physical dissipation, since it generates non-negative dissipation although there is a room for considerable improvements concerning the formulation of dissipation sensors and higher order boundary conditions for artificial dissipation terms. The PBD formulation was only one user specified parameter which can be kept constant over a wide range of Mach numbers.

ACKNOWLEDGEMENTS

The authors would like to thank Ms. Amy Myers for her expert typing of this paper and to Dr. Thomas Pulliam and Dr. Marshall Merriam of the NASA Ames Research Center for their helpful discussions concerning the PBD formulation for Euler and Navier-Stokes equations.

REFERENCES

[1] Jameson, A., Schmidt, W. and Turkel, E., "Numerical Solutions of the Euler Equations by Finite Volume Methods Using Runge-Kutta Time-Stepping Schemes," AIAA Paper No. 81-1259, Palo Alto, CA, June 1981.

[2] Pulliam, T. H., "Artificial Dissipation Models for the Euler Equations," AIAA Journal, Vol. 24, No. 12, December, 1986, pp. 1931-1940.

[3] Caughey, D. A., Private communications, Oct. 1988.

[4] Raj, P. and J. Brennan, "Improvements to an Euler Aerodynamic Method for Transonic Flow Analysis," AIAA paper 87-0040, Reno, NV, Jan. 12-15, 1989.

[5] Raj, P., J. Keen and S. Singer, "Applications of an Euler Aerodynamic Method to Free-Vortex Flow Simulation," AIAA paper CP-88-2517, AIAA Applied Aerodynamics Conf., Williamsburg, VA, June 6-8, 1988.

[6] Salas, M. D., "Recent Developments in Transonic Euler Flow Over a Circular Cylinder," presented at the 10th IMACS World Congress in Systems Simulation and Scientific Computation, Montreal, Canada, August 8-13, 1982.

[7] Abdy, G. L., "Inviscid Separation at Transonic Speeds," M.Sc. Thesis, Dept. of Mechanical and Aerospace Engr., Arizona State Univ., Tempe, AZ, December 1986.

[8] Ni, Ron-Ho, "A Multiple Grid Scheme for Solving the Euler Equations," AIAA Paper No. 81-1025.

[9] Dulikravich, G. S., Dorney, D. J. and Lee, S., "Iterative Acceleration and Physically Based Dissipation for Euler Equations of Gasdynamics," presented at ASME WAM 1988 Symposium on Advances and Applications in Computational Fluid Dynamics, Chicago, IL, Nov. 28-Dec. 2, 1988.

[10] Dorney, D. J. and Dulikravich, G. S. K. D. Lee, "A Comparative Study of Iterative Algorithms for the Euler Equations of Gasdynamics," AIAA paper No. 89-0114, Reno, NV, Jan. 9-12, 1989.

[11] Dulikravich, G. S., Dorney, D. J. and and Lee, S., "Artificial Dissipation Sensors in Computational Gasdynamics," AIAA paper No. 89-0643, Reno, NV, Jan. 9-12, 1989.

[12] Dulikravich, G. S., Mortara, K. W. and Marraffa, L., "A Physically Consistent Model for Artificial Dissipation in Transonic Potential Flow Computations," AIAA paper 88-3654, presented at the First National Congress on Fluid Dynamics, Cincinnati, OH, July 24-28, 1988.

[13] Dulikravich, G. S. and Kennon, S. R., "Theory of Compressible Irrotational Flows Including Heat Conductivity and Longitudinal Viscosity," Int. J. of Math. and Comput. Model., Vol. 10, No. 8, 1988, pp. 583-592.

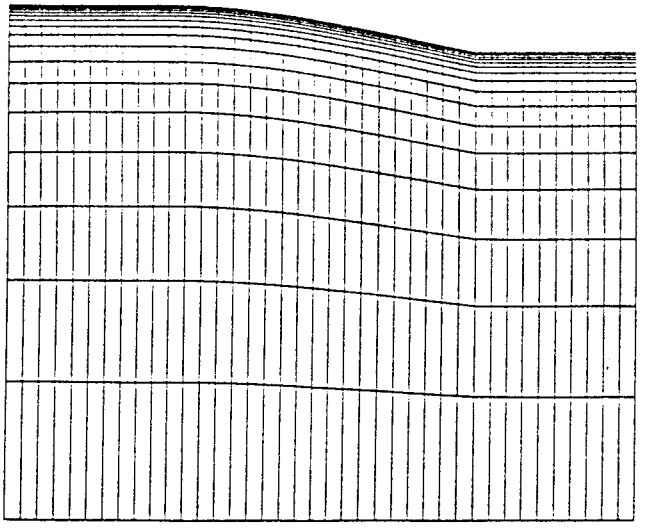

Fig.1 Coarse clustered grid (40 x 20)

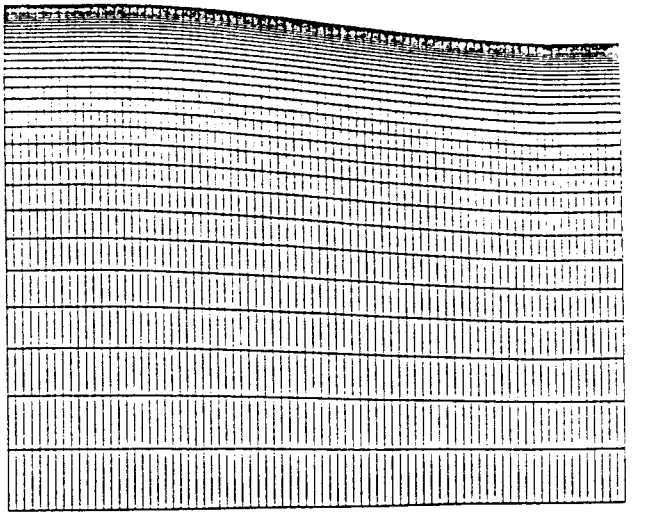

Fig.2 Fine clustered grid (80 x 40)

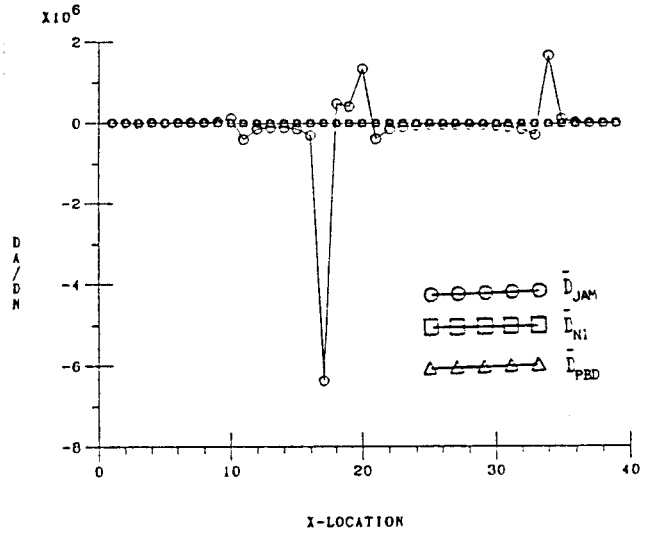

Fig.3 x-momentum dissipation ratios; M_∞=0.60, mid-channel grid line, coarse clustered grid

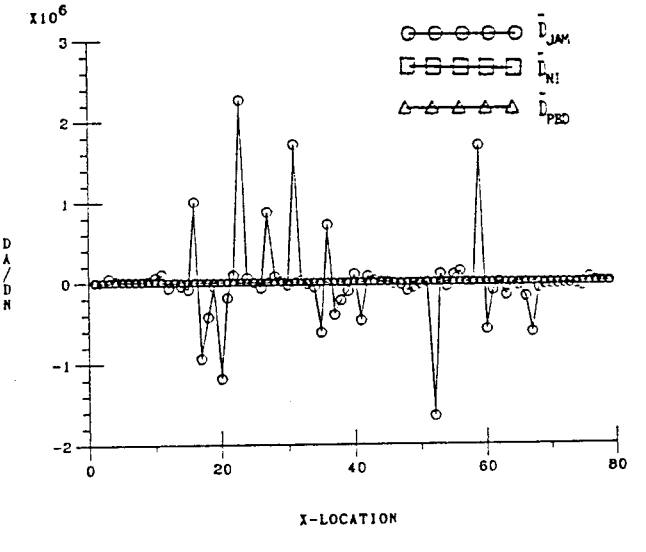

Fig.4 x-momentum dissipation ratios; M_∞=0.60, mid-channel grid line, fine clustered grid

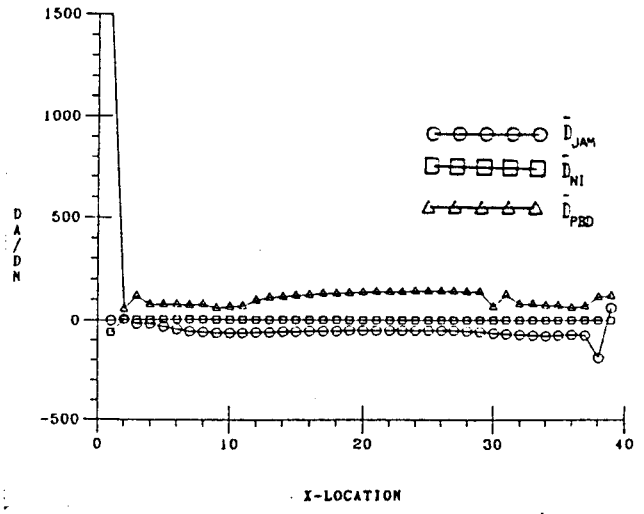

Fig.5 x-momentum dissipation ratios; M_∞=0.60, channel wall grid line, coarse clustered grid

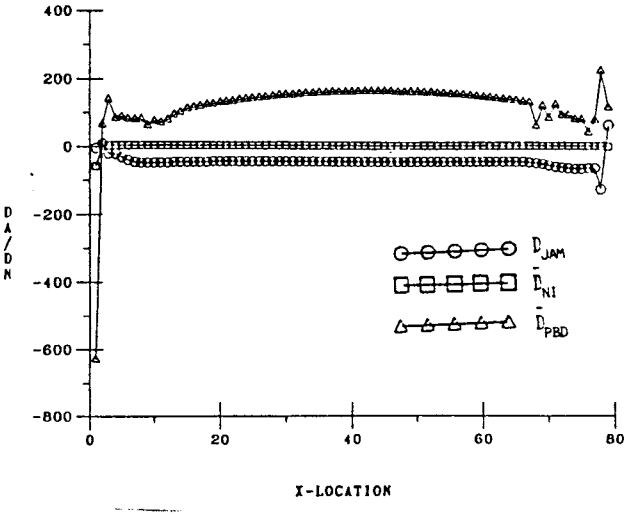

Fig.6 x-momentum dissipation ratios; M_∞=0.60, channel wall grid line, fine clustered grid

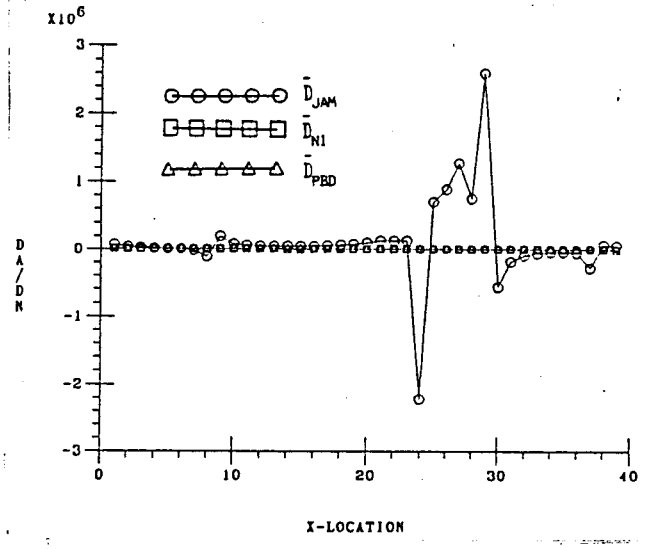

Fig.7 Energy dissipation ratios; M_∞=0.60, mid-channel grid line, coarse clustered grid

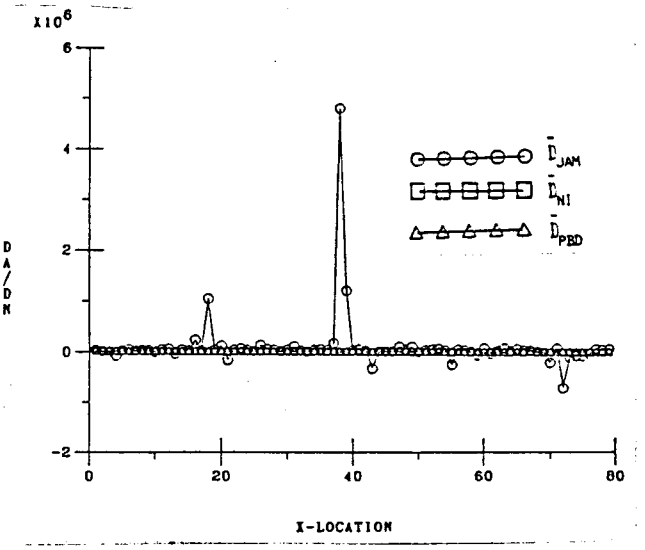

Fig.8 Energy dissipation ratios; M_∞=0.60, mid-channel grid line, fine clustered grid

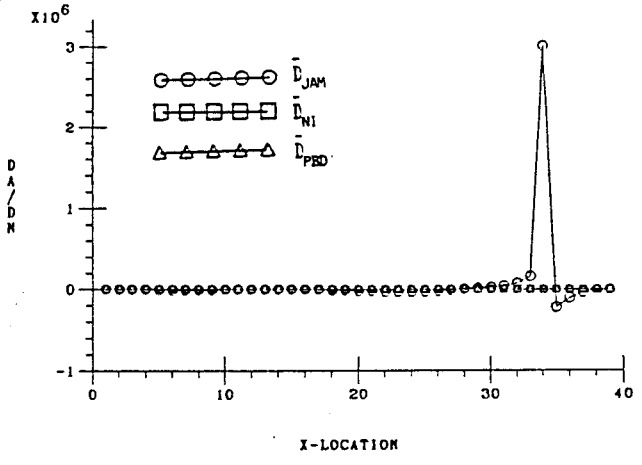

Fig.9 Energy dissipation ratios; M_∞=0.60, channel wall grid line, coarse clustered grid

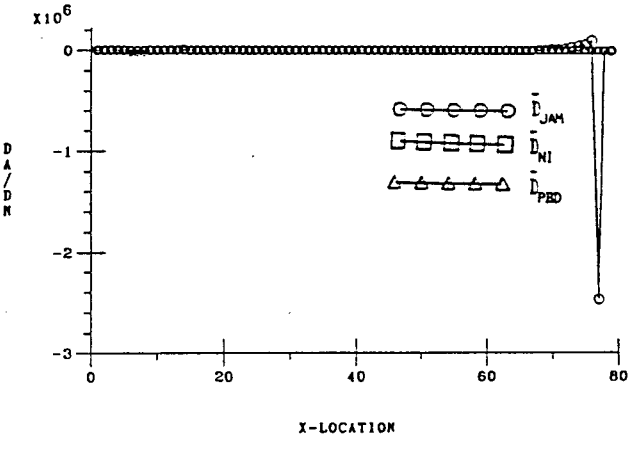

Fig.10 Energy dissipation ratios; M_∞=0.60, channel wall grid line, fine clustered grid

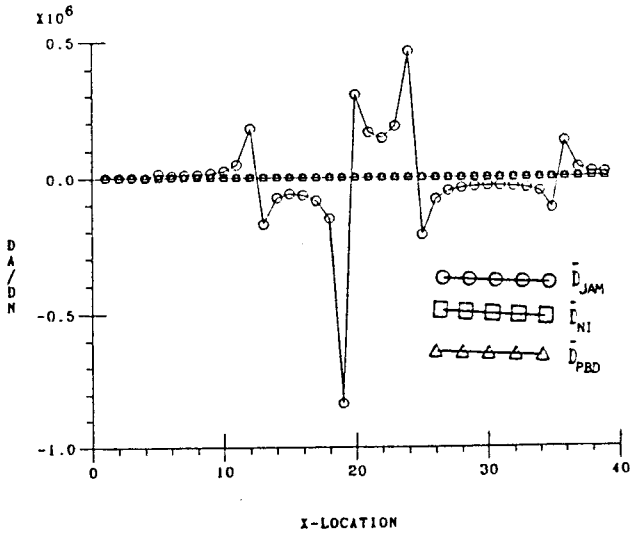

Fig.11 x-momentum dissipation ratios; M_∞=0.90, mid-channel grid line, coarse clustered grid

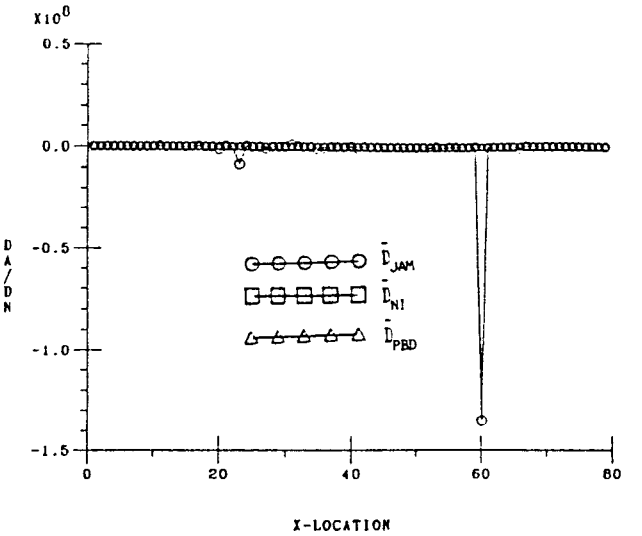

Fig.12 x-momentum dissipation ratios; M_∞=0.90, mid-channel grid line, fine clustered grid

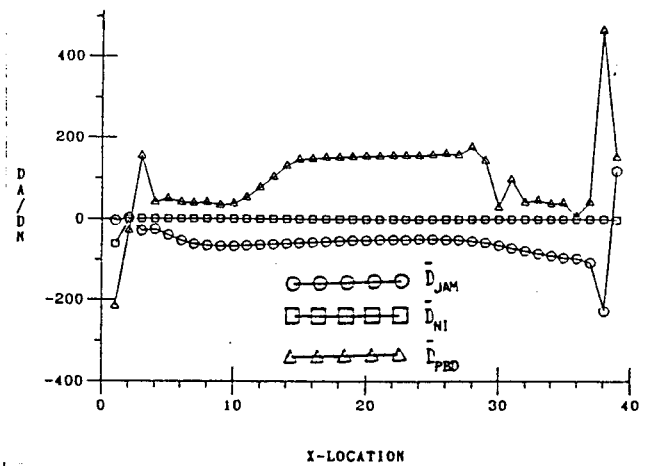

Fig.13 x-momentum dissipation ratios; M_∞=0.90, channel wall grid line, coarse clustered grid

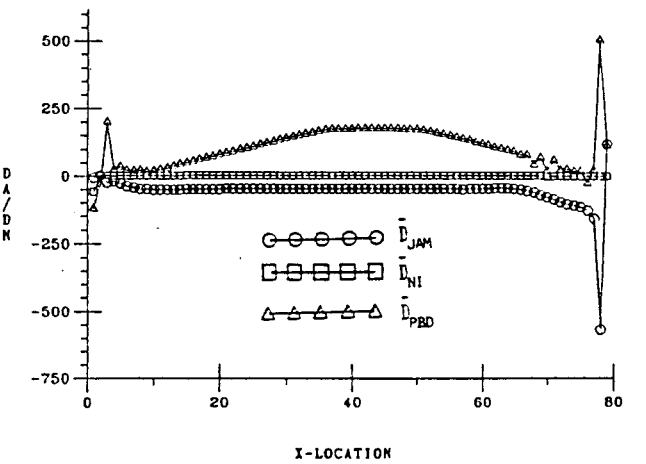

Fig.14 x-momentum dissipation ratios; M_∞=0.90, channel wall grid line, fine clustered grid

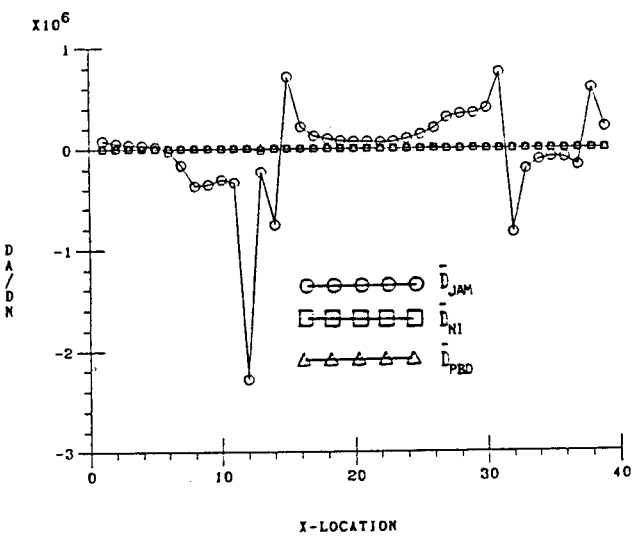

Fig.15 Energy dissipation ratios; M_∞=0.90, mid-channel grid line, coarse clustered grid

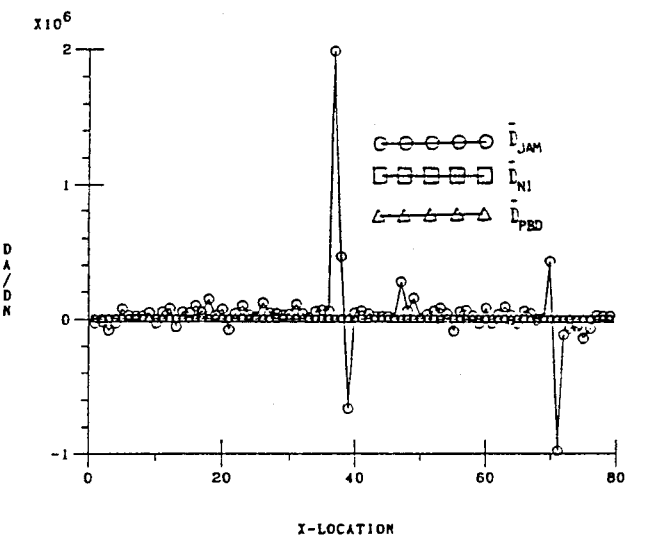

Fig.16 Energy dissipation ratios; M_∞=0.90, mid-channel grid line, fine clustered grid

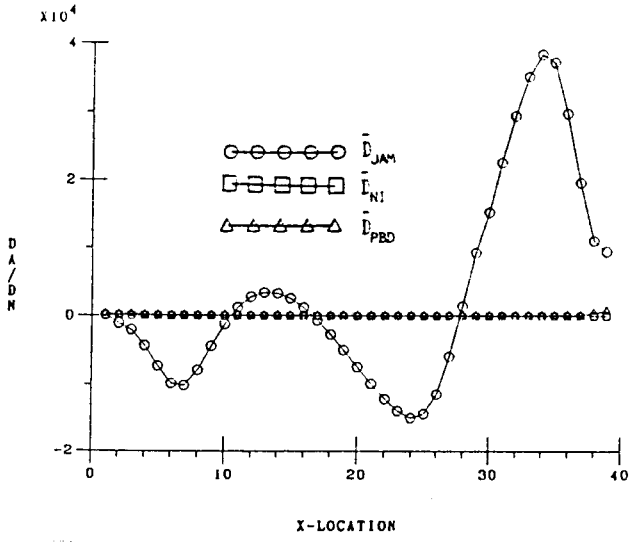

Fig.17 Energy dissipation ratios; M_∞=0.90, channel wall grid line, coarse clustered grid

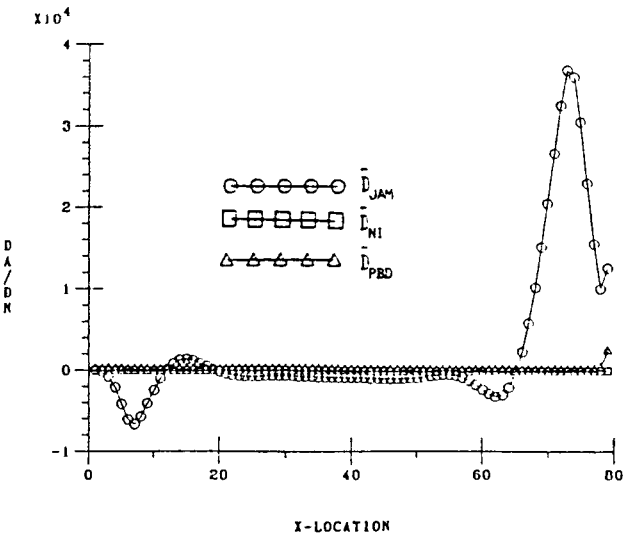

Fig.18 Energy dissipation ratios; M_∞=0.90, channel wall grid line, fine clustered grid

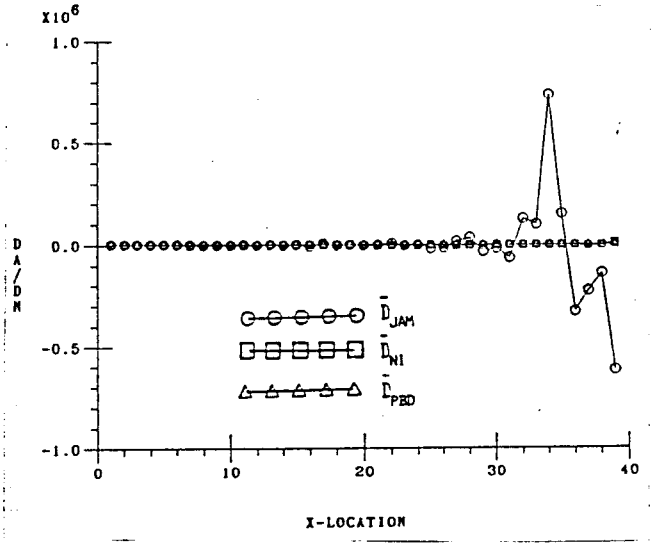

Fig.19 x-momentum dissipation ratios; M_∞=1.2, mid-channel grid line, coarse clustered grid

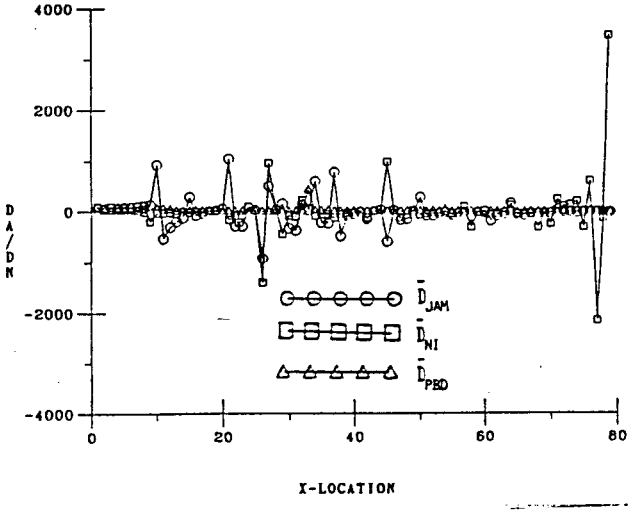

Fig.20 x-momentum dissipation ratios; M_∞=1.2, mid-channel grid line, fine clustered grid

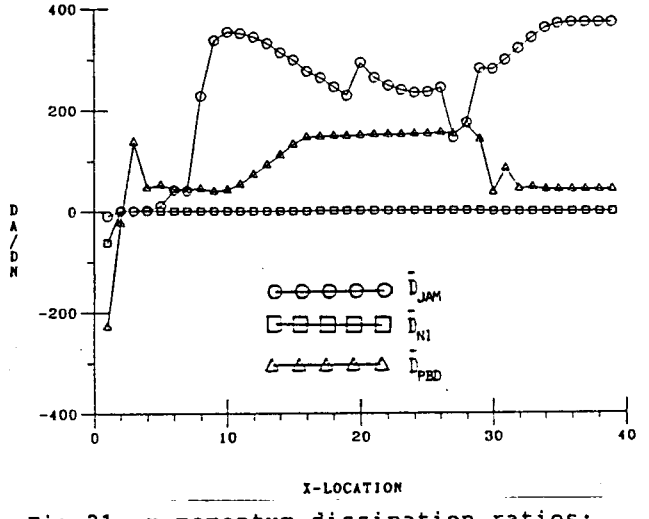

Fig.21 x-momentum dissipation ratios; M_∞=1.2, channel wall grid line, coarse clustered grid

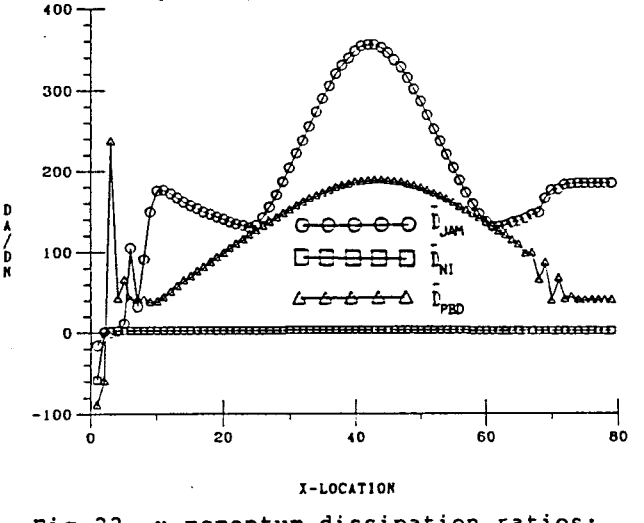

Fig.22 x-momentum dissipation ratios; M_∞=1.2, channel wall grid line, fine clustered grid

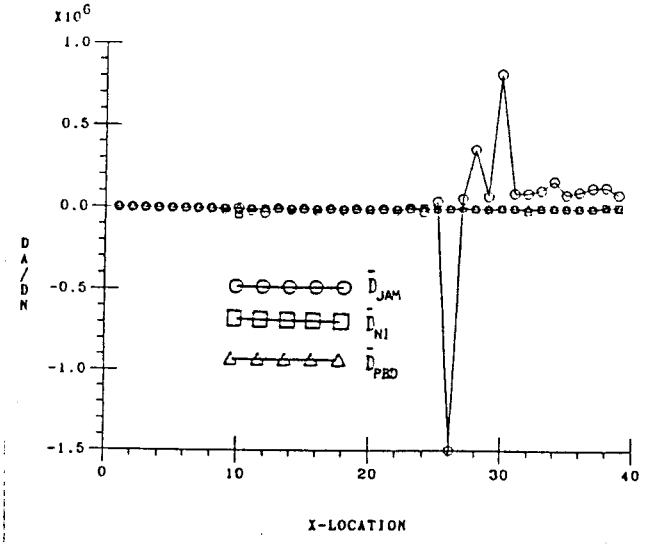

Fig.23 Energy dissipation ratios; M_∞=1.2, mid-channel grid line, coarse clustered grid

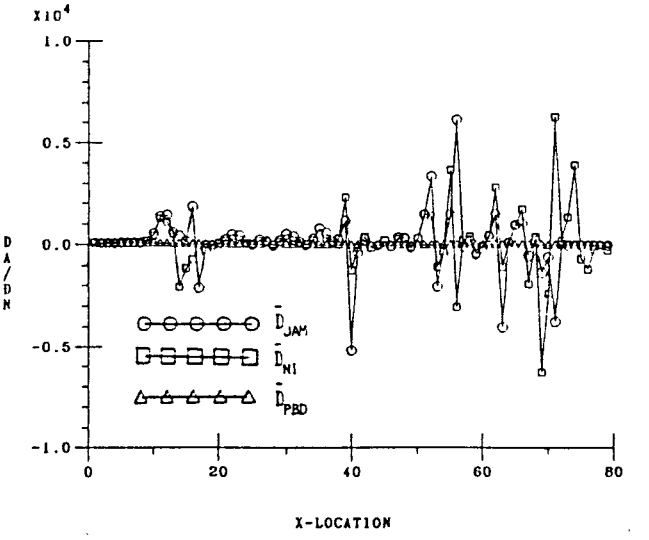

Fig.24 Energy dissipation ratios; M_∞=1.2, mid-channel grid line, fine clustered grid

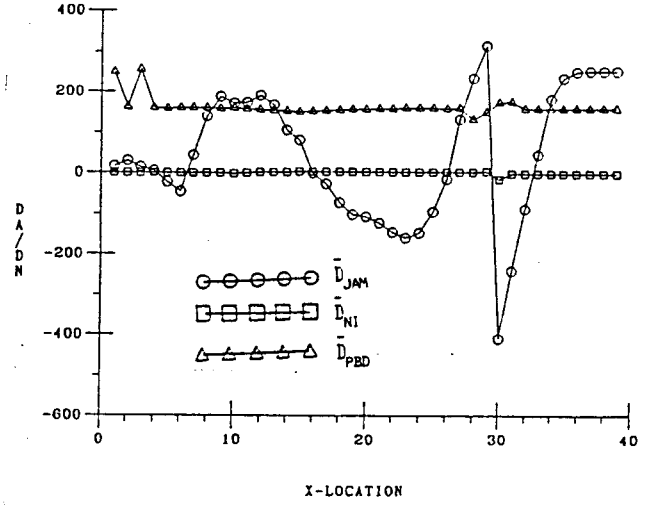

Fig.25 Energy dissipation ratios; M_∞=1.2, channel wall grid line, coarse clustered grid

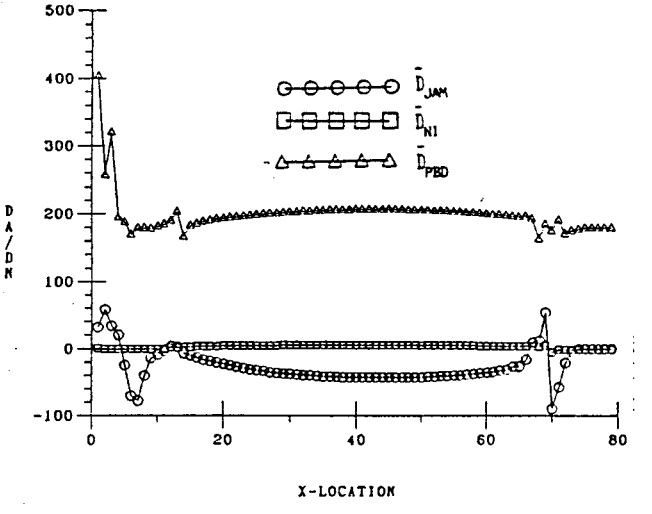

Fig.26 Energy dissipation ratios; M_∞=1.2, channel wall grid line, fine clustered grid

Fig.27 Isobars for M_∞=0.90; fine grid and Jameson's artificial dissipation

Fig.28 Isobars for M_∞=0.90; fine grid and Ni's artificial dissipation

Fig.29 Isobars for M_∞=0.90; fine grid and PBD formulation

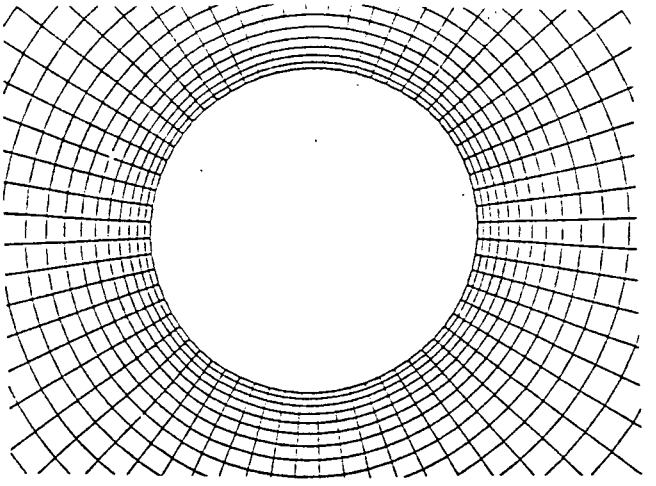

Fig.30 Detail of the computational grid for a circle: (64 x 32) grid cells

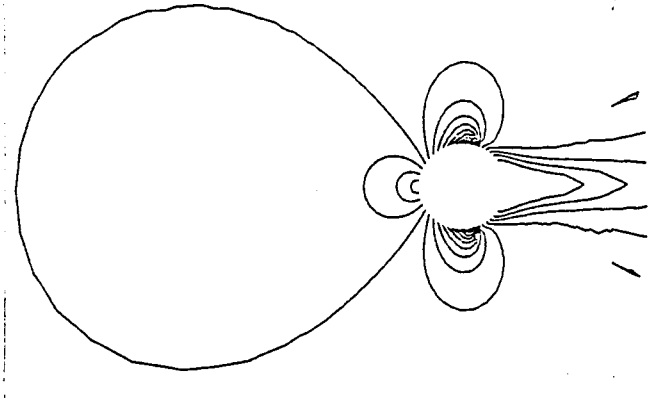

Fig.31 Euler solver: isobars for M_∞=0.5 and Jameson's artificial dissipation

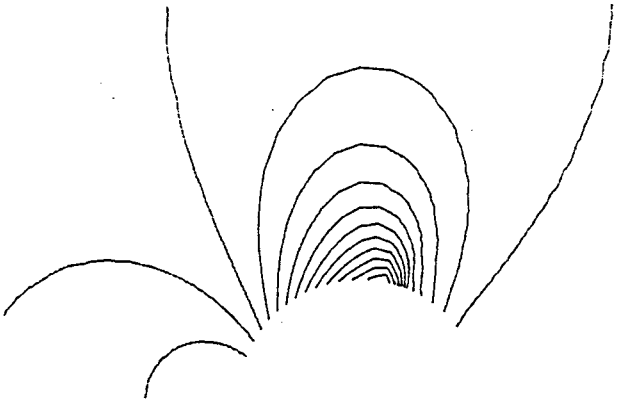

Fig.32 Euler solver: isobars for M_∞=0.5 and PBD formulation

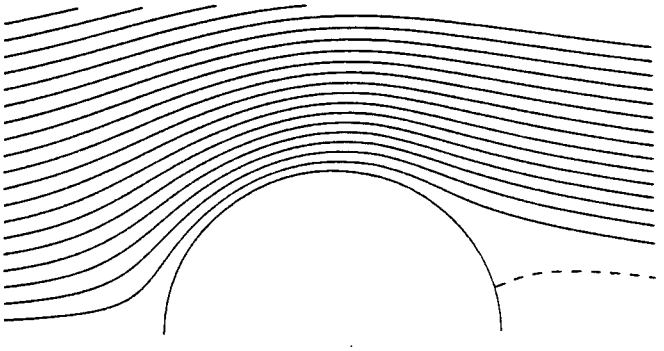

Fig.33 Euler solver: streamlines for M_∞=0.5 and Jameson's artificial dissipation

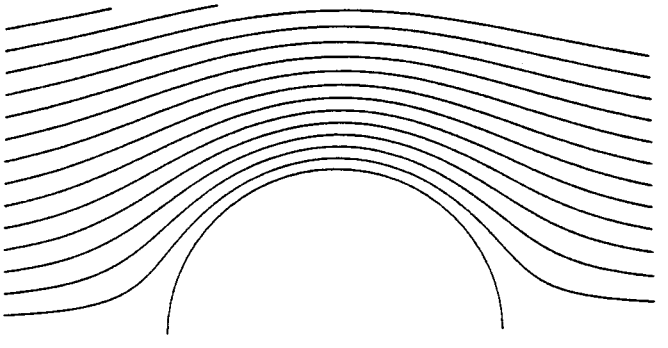

Fig.34 Euler solver: streamlines for M_∞=0.5 and PBD formulation